

# Supported noble metal catalyst with a core-shell structure for enhancing hydrogenation performance

Ningyue Lu, Jiaxin Zhao, Qi Dong, Yanpeng Zhao, Binbin Fan\*

College of Chemistry and Chemical Engineering, Taiyuan University of Technology, Taiyuan, 030024, PR China

## ARTICLE INFO

### Keywords:

Core-shell structure  
Acid sites  
Spillover hydrogen  
Naphthalene

## ABSTRACT

Supported noble metal nanoparticles are a kind of high efficiency of catalysts in aromatics hydrogenation, and the properties and structures of supports are of great importance to improve hydrogenation behaviors. In this work, an efficient Pd/S-1@ZSM-5 core-shell catalyst with an enhanced naphthalene hydrogenation ability was prepared by building acidic nano-ZSM-5 shells surrounding silicalite-1 supported Pd NPs. The acidic nano-ZSM-5 shell can strengthen the spillover hydrogenation due to the increase of the strong acid sites around Pd NPs, and the strong acid sites around metal NPs can be regulated by controlling the coverage of nano-ZSM-5 shell. Additionally, the formed mesoporous structure of nano-ZSM-5 shell is beneficial for the diffusion of bulky reactants. These are the two important factors for enhancing hydrogenation ability of Pd/S-1@ZSM-5 catalyst. Furthermore, Pd/S-1@ZSM-5 catalyst also shows good sulfur-tolerance in the presence of thionaphthene. This work presents an elegant example for enhancing hydrogenation abilities of noble metal catalysts by constructing a core-shell structure.

## 1. Introduction

Aromatics hydrogenation is an industrially important reaction, and the hydrogenated products derived from aromatics have various applications [1–5]. Tetralin, as one of the extended products of naphthalene, is a very useful high boiling point solvent, and has been widely used in paint, pharmaceuticals, hydrogen donors and other fields [6,7]. In addition, with increasingly severe environment and fuel legislation and growing demand for the transportation fuels with a high quality, catalytic hydrogenation of aromatics in diesel fuel is of great practical significance for upgrading fuel quality [1,8]. Aromatics hydrogenation is an exothermic reaction and thus thermodynamically favored at low temperatures. Thus, compared to the conventional Co-Mo and Ni-Mo sulfides with weak hydrogenation abilities at low temperature, noble metal catalysts are more favorable [9,10].

Supported noble metal nanoparticles (NPs), as a significant class of catalysts, have been extensively applied in various industrial reactions. The catalytic performances of the supported catalysts are dependent on the physicochemical properties of the supported metal NPs, its surface property and pore structure as well as the interaction between metal NPs and the supports [11–15]. Zeolites with well-defined channels and facilely adjustable acid-base properties, are widely employed as

supports for metal NPs, and zeolite supported noble metal catalysts, due to their high hydrogenation activities, are promising candidates for deep aromatics hydrogenation at lower temperatures [16–18].

In hydrogenation reactions over supported noble metal catalysts, the acidity of the supports greatly influences the hydrogenation performances of the supported catalysts. Generally, acid supported noble metal catalysts show activity enhancements compared with non-acid supported metal catalysts, especially in hydrogenation. This is due to that hydrogenation activities obtained over the acid supported noble metal catalysts are mainly contributed by two parts: one is the metal-catalyzed hydrogenation, and the other is spillover hydrogenation [19–22]. In the process of spillover hydrogenation, the adsorbed aromatic compound can be hydrogenated through spillover hydrogen, which is formed on the metal sites and migrates onto acid sites in the interfacial region between metal and acid sites [23,24]. In our previous work on naphthalene hydrogenation over Pt/HZSM-5 and the related literatures [19,25], the contribution from spillover hydrogenation greatly affects the hydrogenation ability of the supported noble metal catalysts, and the acid amounts with proximity to the metal play a decisive role for spillover hydrogenation. However, in the zeolite supported metal catalysts prepared by the conventional supporting methods, such as wetting impregnation and ion-exchange, the supported

\* Corresponding author.

E-mail address: [fanbinbin@tyut.edu.cn](mailto:fanbinbin@tyut.edu.cn) (B. Fan).

<https://doi.org/10.1016/j.mcat.2021.111543>

Received 23 December 2020; Received in revised form 4 March 2021; Accepted 20 March 2021

Available online 5 April 2021

2468-8231/© 2021 Elsevier B.V. All rights reserved.

metal nanoparticles (NPs) are mainly located on the external surface of the zeolite supports upon calcination and reduction, while the acid sites are mainly located in the zeolite channels. As a consequence, the acid amounts with a proximity to the supported metal NPs are very limited, greatly restricting the enhancement of the hydrogenation ability of the zeolite-supported metal catalysts [26]. Hence, the rational design and preparation of aromatics hydrogenation catalysts with an appropriate metal/acid matching relationship is still a challenge. In addition, for zeolite-supported catalysts, it is difficult to individually evaluate the effects of the acidity of the zeolite supports on hydrogenation reactions because the acidity not only can influence the dispersions and electronic states of the supported metal species, but also the acid sites on the supports can induce spillover hydrogenation. Thus, in order to understand the influences of the acidity of the supports on hydrogenation reactions, it is also desirable to design appropriate catalysts.

Encapsulation of metal NPs inside zeolite has been developed as a powerful strategy for preparing intriguing catalysts with the distinct selectivity, activity as well as stability (against sintering) [27–36]. Meanwhile, enhancing proximity of the acid sites to the supported metal NPs is one of the significant features of zeolite-encapsulated metal NPs [37–39]. Depending on Si/Al ratios, pore sizes of the zeolite hosts and stability/size of the metal precursors, many approaches, including host-guest assembling of metal precursors inside the zeolites, re-transformation, in-situ encapsulation involving ligand-stabilized methods or precursor-stabilization methods and shell-caged methods, have been developed for encapsulating metal NPs inside zeolites [40–44]. However, zeolite hosts, especially the small-aperture zeolites, generally exert heavy diffusion limitations on the reactions involving bulky substrates and products due to the steric restriction from zeolite channels.

Similar to zeolite-encapsulated catalysts, core-shell catalysts, in which the metal NPs are totally encapsulated in zeolite shells formed by zeolite nanocrystals, are also an attractive class of materials and have received much attention in the last few years due to combining the properties of the metal with those of the zeolite membrane [26,45–48]. Zeolite shell not only can increase the sintering-resistant of the encapsulated metal NPs and endow core-shell catalysts with the shape selective properties, but also can maximize the contact between metal and zeolite supports. In addition, the mesoporous structure of the zeolite shell can also improve the diffusion limitation. Therefore, core-shell catalysts provide an insight and possibility for design and preparation of the catalyst with enhanced hydrogenation ability in the reactions involving bulky substrates. However, the work on this field is rarely reported.

Herein, we design an efficient hydrogenation core-shell catalyst by constructing the acidic nano-ZSM-5 shell around silicalite-1 supported Pd NPs core (Pd/S-1@ZSM-5). The core-shell catalysts have the following features: acidic nano-ZSM-5 shell increases the acid sites with a high proximity to the encapsulated metal NPs, and strengthens the spillover hydrogenation; nano-ZSM-5 shell can form mesoporous structure, which is beneficial for the accessibility of the encapsulated metal NPs to bulky reactants; the acidic nano-ZSM-5 shell can protect the noble metal from poisoning by organic sulfide to some extent in naphthalene hydrogenation (model compound of light cycle oil). In addition, the designed catalyst is also of interest for individually exploring the influences of the acidity of the zeolite supports on the hydrogenation performance of the zeolite-supported metal catalysts by only changing the acid amounts with a proximity to metal via regulating the coverage of the zeolite shells.

## 2. Experimental

### 2.1. Sample synthesis

#### 2.1.1. Silicalite-1 (S-1)

Silicalite-1 was synthesized from a synthesis gel with the molar

composition of 1 SiO<sub>2</sub>: 0.3 TPABr: 0.2 NaOH: 100 H<sub>2</sub>O. In a typical experiment, 2.24 g tetrapropylammonium bromide (TPABr) and 0.22 g NaOH were dissolved in 50 mL deionized H<sub>2</sub>O, and then 6.3 mL TEOS was dropwise added to the solution. After the mixture was homogenized by vigorous magnetic stirring at ambient temperature for 4 h, it was transferred into a 100 mL Teflon-lined steel autoclave and crystallized at 160 °C for 2 days. The obtained solid was washed with deionized H<sub>2</sub>O, dried at 100 °C overnight, and calcined at 550 °C for 6 h in air atmosphere. The resultant final product was denoted as S-1.

#### 2.1.2. Pd/S-1

Pd/S-1 was synthesized according to the following procedures. 1 g S-1 and 1 mL 3-aminopropyltrimethoxysilane (APTMS) were added into the flask with 30 mL dichloromethane, and then the mixture was stirred for 24 h at room temperature. After the white solid was filtered, washed with dichloromethane and dried under vacuum, APTMS-functionalized S-1 was obtained. The obtained APTMS-functionalized S-1 was added into the 5 mL Na<sub>2</sub>PdCl<sub>4</sub> aqueous solution (0.05 mol/L) and the mixture was stirred at room temperature for 24 h. Afterwards, 10 g tetrapropylammonium hydroxide water solution (TPAOH, 15 wt%) was dropwise into the above resulting mixture and transferred into a 50 mL Teflon-lined autoclave. After hydrothermal treatment at 160 °C for 24 h, the solid products were collected by centrifugation, washed with deionized water to dislodge excess amount of TPA<sup>+</sup> and OH<sup>-</sup> and dried at 100 °C. Finally, the powder was added in the 50 mL sodium borohydride solution (0.15 mol/L), and the mixture was stirred for 6 h to ensure the reduction of Pd<sup>2+</sup>.

#### 2.1.3. Pd/S-1@ZSM-5

Pd/S-1@ZSM-5 with a core-shell structure was prepared by epitaxial growth. Typically, 1 g TPABr, 0.034 g NaAlO<sub>2</sub> and 0.085 g NaOH were dissolved in the 20 mL deionized H<sub>2</sub>O in turn, and 2.1 g TEOS was dropwise added to the above solution to form synthesis gel of ZSM-5 with the molar composition of 1 SiO<sub>2</sub>: 0.014 Al<sub>2</sub>O<sub>3</sub>: 0.37 TPABr: 0.25 NaOH: 110 H<sub>2</sub>O. Then 1 g Pd/S-1 was added into synthesis gel of ZSM-5 and treated by ultrasonic for 30 min. The formed mixture was transferred to a Teflon-lined steel autoclave and crystallized at 180 °C for a period of time. The obtained solid product was calcined at 550 °C for 6 h in an air atmosphere and denoted as Pd/S-1@ZSM-5-x (x = crystallization time (h)). Pd/S-1@HZSM-5-x was prepared by ion-exchange of the corresponding Pd/S-1@ZSM-5-x with NH<sub>4</sub>NO<sub>3</sub> solution (1 mol/L) three times at 80 °C for 2 h, and then calcined at 550 °C for 4 h. In addition, based on the synthesis of Pd/S-1@ZSM-5–48 sample, Pd/S-1@ZSM-5–48-1 and Pd/S-1@ZSM-5–48-2 with different Si/Al atomic ratios were synthesized by adjusting the amounts of NaAlO<sub>2</sub> in synthesis gel of ZSM-5 shell.

#### 2.1.4. Preparation of the reference samples

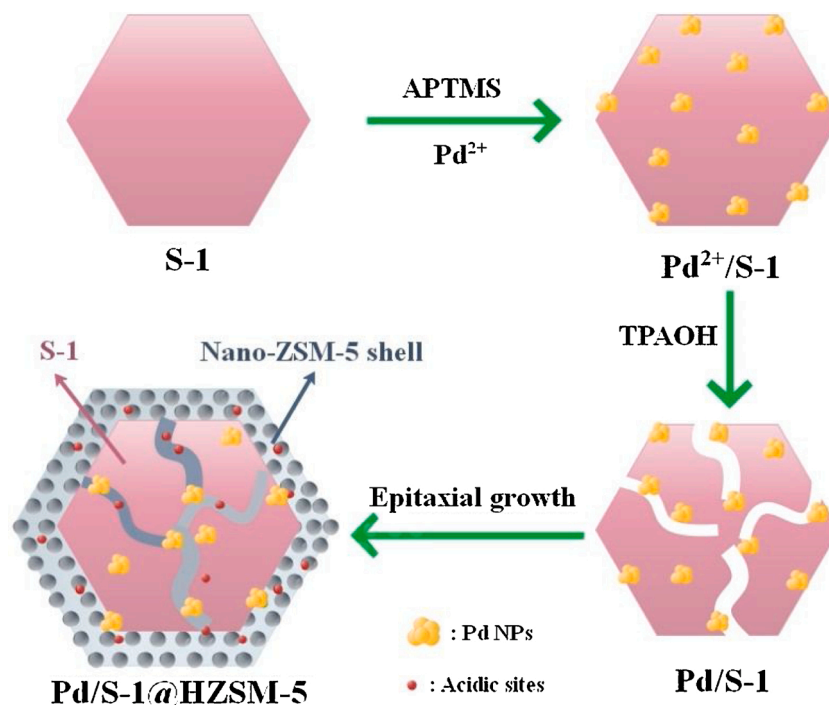
Pd/S-1@NaZSM-5–48 was prepared by ion-exchange of Pd/S-1@ZSM-5–48 with NaCl solution (1 mol/L) three times at 80 °C for 2 h and calcination at 550 °C for 4 h. S-1@HZSM-5–48 was synthesized according to the preparation procedure of S-1@HZSM-5–48 without the addition of Pd source, and Pd/[S-1@HZSM-5–48] was prepared by conventional incipient wetness impregnation with S-1@HZSM-5–48 as the support. Pd contents in Pd/[S-1@HZSM-5–48] are 0.63 wt% (ICP analysis). Pd/S-1+HZSM-5 was obtained by physically mixing Pd/S-1 with HZSM-5 in a certain mass proportion, in which the Pd and HZSM-5 contents are similar to Pd/S-1@HZSM-5–48. Pd/HZSM-5 with a similar acid property and Pd content to Pd/S-1@HZSM-5–48 was prepared by incipient wetness impregnation.

## 2.2. Characterization

X-ray powder diffraction (XRD) patterns were recorded on a Shimadzu XRD-6000 diffractometer with Cu K $\alpha$  radiation. Nitrogen adsorption/desorption isotherms were measured on a Quantachrome NOVA 1200e



Scheme 1. The reaction route for the naphthalene hydrogenation.



Scheme 2. The preparation procedure for Pd/S-1@ZSM-5.

apparatus at  $-196\text{ }^\circ\text{C}$ . The samples were evacuated at  $300\text{ }^\circ\text{C}$  for 3 h prior to measurement. Scanning electron microscope (SEM) images were conducted on a Hitachi S-4800 scanning electron microscope operating at 20 kV. Transmission electron microscopy (TEM) measurement was conducted on a JEOL JEM-2100 F electron microscope operating at 200 kV. The ammonia temperature programmed desorption ( $\text{NH}_3$ -TPD) was measured on a XIAN QUAN TP-5076 dynamic adsorption apparatus. Metal contents were measured by inductively coupled plasma-atomic emission spectrometer (ICP-AES, Autoscan16 TJA). X-ray photoelectron spectra (XPS) were attained on a Kratos AXIS ULTRA DLD XPS spectrometer with a monochromated Al  $K\alpha$  target. The binding energies were calibrated by the C 1s peak at 284.8 eV as the reference.  $\text{H}_2$  chemisorption was carried out on the Micromeritics AutoChem II 2920. Sample (100 mg) was reduced with 10 %  $\text{H}_2/\text{Ar}$  at  $350\text{ }^\circ\text{C}$  for 2 h and purged in Ar for 1 h. Then the temperature was cooled to  $30\text{ }^\circ\text{C}$ ,  $\text{H}_2$  pulses were performed by a calibrated on-line sampling valve. The calculation was based on a H/Pd stoichiometry of 1.

### 2.3. Catalytic measurement

Naphthalene hydrogenation (Scheme 1) over the different samples was performed on a micro and high-pressure fixed bed reactor ( $12\text{ mm} \times 2\text{ mm} \times 500\text{ mm}$ ). 200 mg sample was diluted with quartz sand and loaded in the constant temperature zone of the reactor. Prior to the reaction, the samples were in-situ reduced under 1 atm  $\text{H}_2$  ( $90\text{ mL min}^{-1}$ ) at  $350\text{ }^\circ\text{C}$  for 2 h. After reduction, the reactor was cooled to the reaction temperature ( $280\text{ }^\circ\text{C}$ ) and the pressure was raised to 4 MPa. The feed (5 wt% naphthalene in the n-octane solvent) was injected to reactor at a

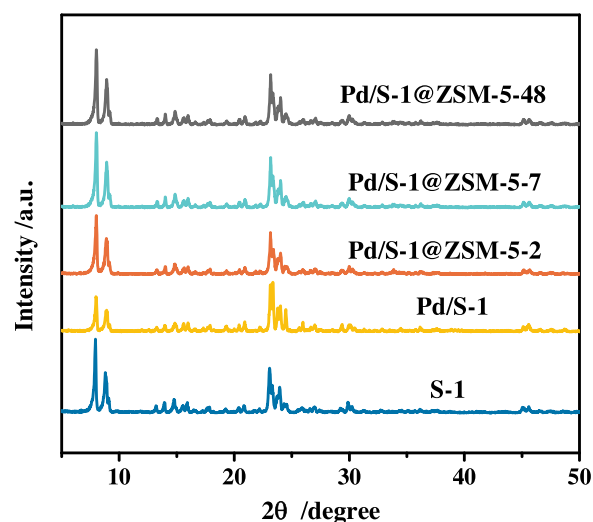


Fig. 1. XRD patterns of the different samples.

rate of  $7.2\text{ mL h}^{-1}$  by micrometer pump and the  $\text{H}_2$  flow was  $90\text{ mL min}^{-1}$ . The liquid products were collected and analyzed off-line by an Agilent 7820A gas chromatograph equipped with a HP-5 capillary column ( $30\text{ m} \times 0.32\text{ mm} \times 0.25\text{ }\mu\text{m}$ ) and a flame ionization detector.

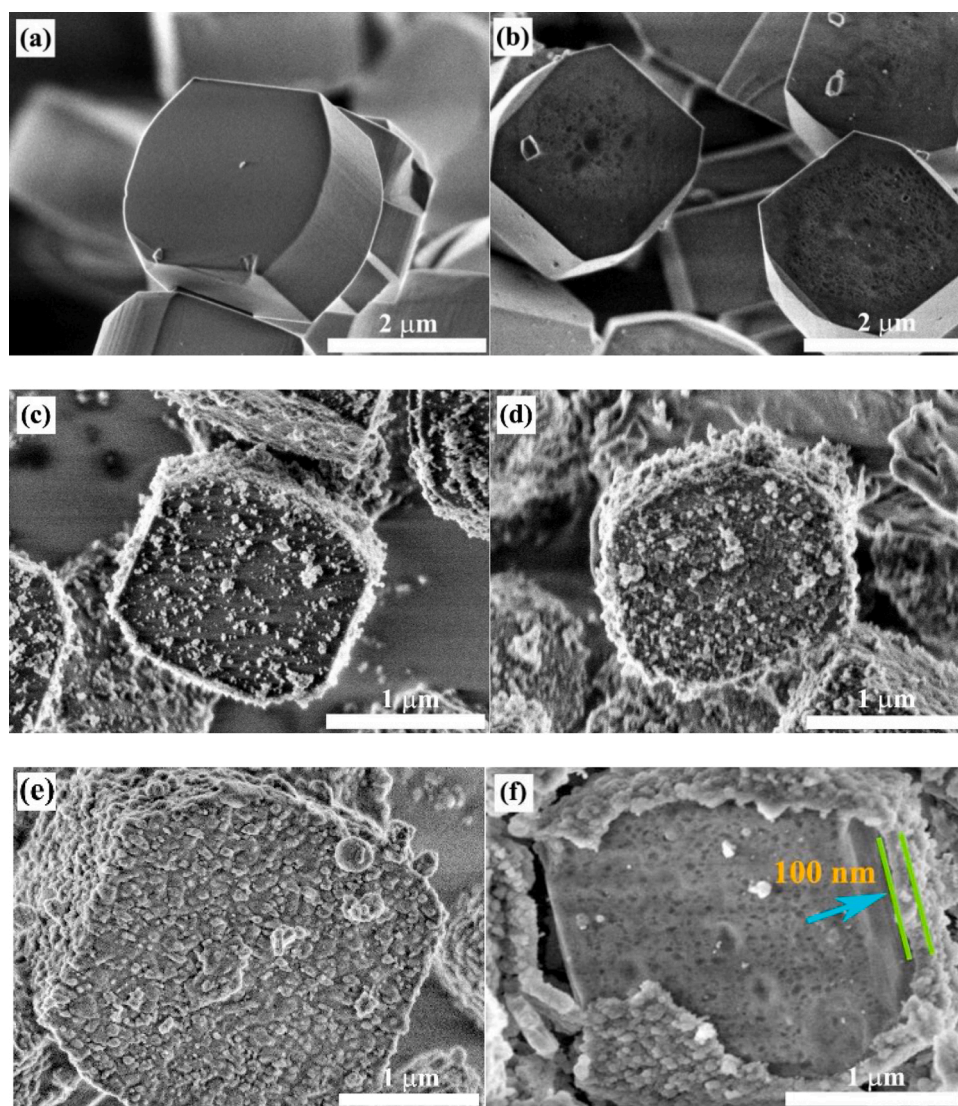


Fig. 2. SEM images of S-1 (a), Pd/S-1 (b), Pd/S-1@ZSM-5-2 (c), Pd/S-1@ZSM-5-7 (d), Pd/S-1@ZSM-5-48 (e), Pd/S-1@ZSM-5-48-broken (f).

### 3. Results and discussion

#### 3.1. Catalyst characterization

Scheme 2 shows the preparing procedure toward Pd/S-1@ZSM-5 core-shell samples. For facile characterization of the core-shell structure and improvement of the dispersion of supported Pd NPs, S-1 composed of regular quadrilateral-like crystals with 2–3 μm in length, 2–3 μm in width and 1–1.5 μm in thickness and functionalized with APTS was used as the core. In order to coat ZSM-5 shell around Pd/S-1 core via epitaxial growth, Pd/S-1 was treated with TPAOH to form the rough surface and more structure defects. Four typical samples with the different coverage of the zeolite shells, termed as Pd/S-1@ZSM-5-x (x denoting the crystallization time in constructing shell), were prepared. The XRD patterns of the different samples are shown in Fig. 1. S-1 exhibits well-resolved diffraction peaks of MFI zeolite. The diffraction peak intensity of Pd/S-1 is weaker than that of S-1, suggesting the zeolite frameworks were partially etched upon hydrothermal treatment with TPAOH. No XRD peaks attributed to Pd phase are observed, indicating the Pd NPs are relatively small and highly dispersed. All the Pd/S-1@ZSM-5-x samples show MFI typical diffraction reflections with the similar reflection intensities to S-1.

Successful coating of ZSM-5 shell over Pd/S-1 core can be confirmed

Table 1

Pd dispersion and acidity properties of the various samples.

Samples	Pd Dispersion (%) <sup>a</sup>	ZSM-5 shell coverage (%) <sup>b</sup>	Area under NH <sub>3</sub> -TPD peaks (a.u./mg) <sup>c</sup>		
			Weak	Medium	Strong
Pd/S-1	12.4	–	1.2 (204.1)	–	0.4 (431.6)
Pd/S-1@ZSM-5-2	11.7	40.9	2.5 (205.7)	0.6 (273.0)	4.4 (362.7)
Pd/S-1@ZSM-5-7	12.7	49.2	2.0 (198.6)	1.3 (264.4)	5.7 (384.1)
Pd/S-1@ZSM-5-48	11.9	53.8	2.2 (201.7)	1.3 (277.9)	6.3 (386.3)

<sup>a</sup> Determined by H<sub>2</sub> chemisorption.

<sup>b</sup> Based on Pt loading.

<sup>c</sup> Determined by NH<sub>3</sub>-TPD (desorption temperature in parenthesis).

by SEM images shown in Fig. 2. As shown in Fig. 2, all the Pd/S-1@ZSM-5-x samples obtained at the different crystallization time show the presence of ZSM-5 shells over Pd/S-1 core. For Pd/S-1@ZSM-5-2, only

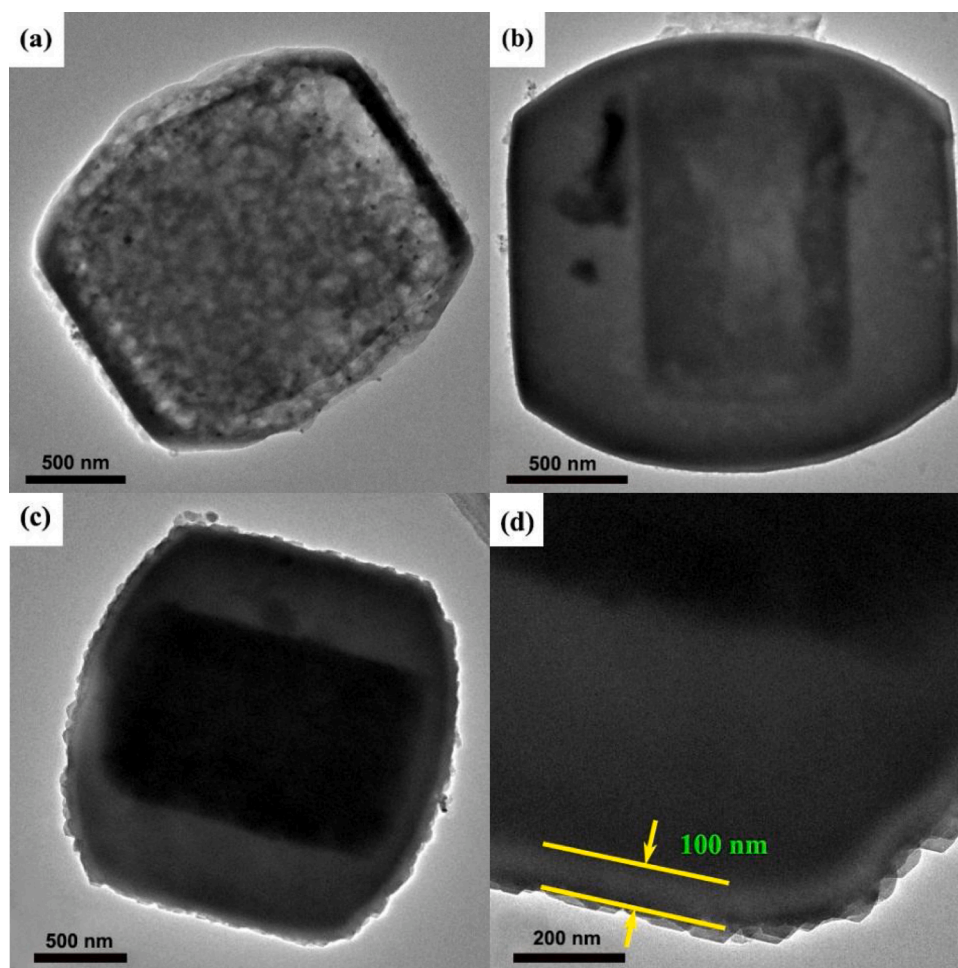


Fig. 3. TEM images of Pd/S-1@ZSM-5-2 (a), Pd/S-1@ZSM-5-7 (b) and Pd/S-1@ZSM-5-48 (c,d).

sparse ZSM-5 nanocrystals are gathered and attached to the surface of Pd/S-1. Upon increasing crystallization time, more ZSM-5 nanocrystals are accumulated on the surface of Pd/S-1 core. A relative integrated shell loosely assembled by ZSM-5 nanocrystals is gradually formed over Pd/S-1 core as the crystallization time is beyond 7 h. With the further extension of crystallization time to 48 h, a completely integrated ZSM-5 shell, composed of ZSM-5 nanocrystals with a size of 50–100 nm, is formed, and its thickness reaches ca. 100 nm (Fig. 2 (f)). The above results indicate the ZSM-5 shell is successfully formed over Pd/S-1 core by the continuous epitaxial growth and the coverage of ZSM-5 nanocrystals on Pd/S-1, that is the integration of the formed shell, can be facilely tailored via controlling crystallization time (Table 1).

The TEM images of Pd/S-1@ZSM-5-x samples are present in Fig. 3. As shown in Fig. 3, Pd NPs in Pd/S-1@ZSM-5-2 are evenly dispersed in the crystal, and the size of Pd NPs are approximately 10 nm, which is similar to that of Pd NPs in Pd/S-1 (Figure S1). However, with the crystallization of ZSM-5 shell, Pd NPs are difficult to be captured for Pd/S-1@ZSM-5-x samples due to the ZSM-5 shell cover. In order to confirm the distribution of Pd NPs, the EDX elemental mapping of Pd/S-1@ZSM-5-48 are measured and shown in Fig. 4, it can be seen that Pd NPs are well dispersed in the Pd/S-1@ZSM-5-48 crystal (Fig. 4). From the H<sub>2</sub> chemisorption results, it can be seen that these Pd/S-1@ZSM-5-x core-shell samples have a similar Pd dispersion to Pd/S-1 (Table 1). In addition, the mesoporous pores were formed in Pd/S-1 upon TPAOH etching, which is favored for coating ZSM-5 shells over Pd/S-1 core, and the mesoporous pores in Pd/S-1 disappear in the process of ZSM-5 shell construction. In the TEM image of Pd/S-1@ZSM-5-48, the ZSM-5 shell with a thickness of 100 nm can be further strongly evidenced by bright

region surrounding the one with darker contrast (Fig. 3d).

The chemical states of Pd NPs on Pd/S-1 and Pd/S-1@HZSM-5-48 were evaluated by XPS analysis, and the results are shown in Fig. 5. For Pd/S-1, two peaks at 335.7 and 341.0 eV assigned to the 3d<sub>5/2</sub> and 3d<sub>3/2</sub> levels of metallic Pd can be observed [26]. Pd/S-1@HZSM-5-48 gave the similar 3d binding energy (BE) values of Pd to Pd/S-1, indicating that the ZSM-5 shell over Pd/S-1 has a little effect on the chemical state of the supported Pd NPs. This is different from the results observed by Chai et al. over zeolite-encapsulated Pd NPs [38]. They found that Pd 3d BE values obviously shifted toward higher values by 0.5–0.6 eV upon encapsulation due to the electron transfer from Pd to zeolite framework. From Fig. 5, it also can be found that the intensities of Pd 3d XPS signals in Pd/S-1@HZSM-5 are much lower than that in Pd/S-1. Except the lower Pd loadings, the Pd NPs in Pd/S-1@HZSM-5-48 are covered by ZSM-5 shell is also another rational reason. This is in accordance with those obtained over zeolite-encapsulated Pd samples reported in the references [38] and provide an indirectly evidences for the successfully constructing core-shell structure.

The N<sub>2</sub> adsorption-desorption isotherms of Pd/S-1 and Pd/S-1@HZSM-5-x samples are shown in Fig. 6. The curve of S-1 displays a type I sorption isotherm, indicating the microporous structure of S-1 (Figure S2). Hysteresis loops appeared at  $p/p_0 = 0.15\sim 0.4$  in the curves of all samples (Fig. 6a and Figure S2) are caused by fluid-to-crystal-like phase transition of N<sub>2</sub> molecules in the micropores [49]. Thus, the mesopores centered at around 2.8 nm in pore diameter curves of all the samples are illusory actually (Fig. 6b). Pd/S-1 displays a lower surface area and microporous volume than S-1, indicating treatment with TPAOH has an effect on the framework of S-1. Treatment S-1 with

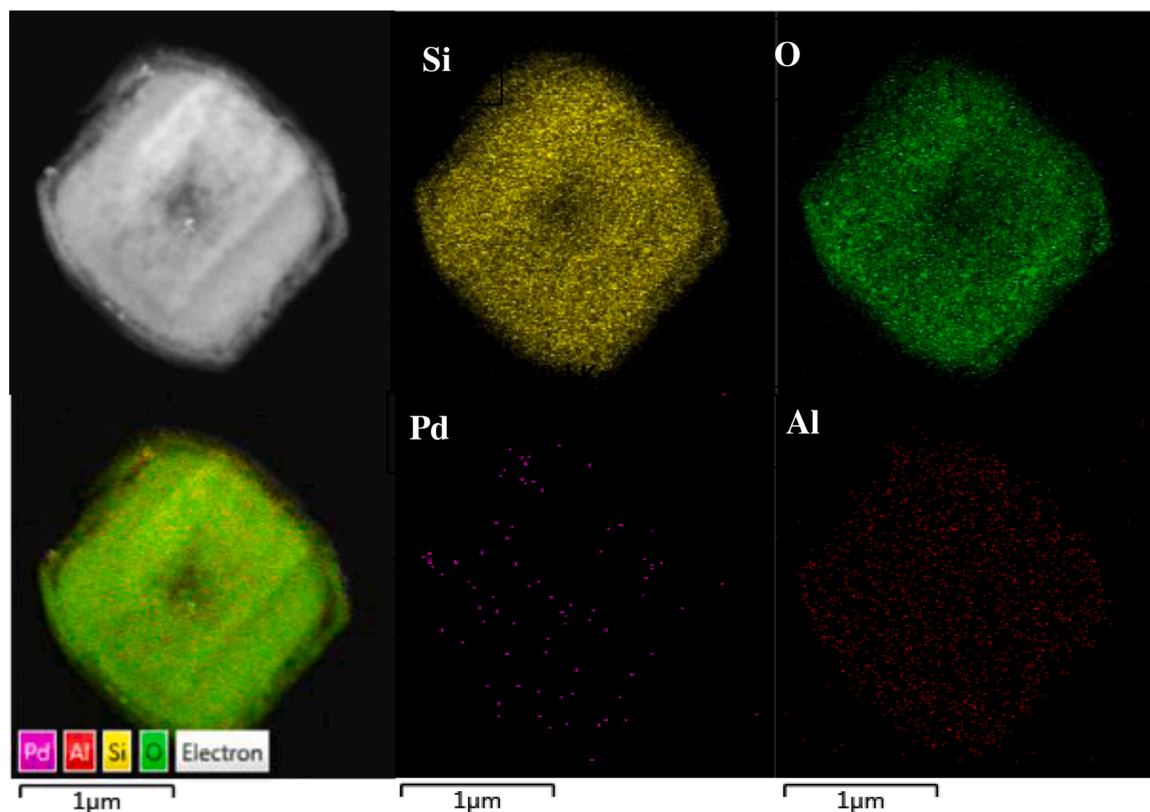


Fig. 4. EDX elemental mapping of Pd/S-1@ZSM-5-48.

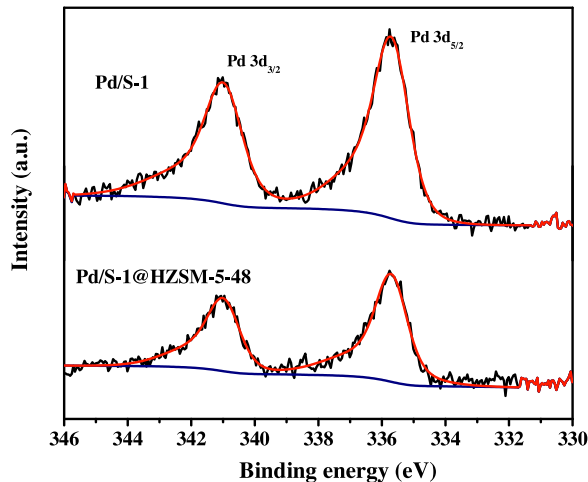


Fig. 5. Pd 3d XPS spectra for Pd/S-1 and Pd/S-1@ZSM-5-48.

TPAOH generates mesoporous in Pd/S-1 crystals, which is evidenced by the presence of hysteresis loop at  $P/P_0 > 0.45$  in the  $N_2$  adsorption-desorption isotherm of Pd/S-1. During constructing ZSM-5 shell over Pd/S-1, the mesoporous volumes of the Pd/S-1@ZSM-5-x samples drop as the increase of secondary crystallization time (Table 2), and basically keep constant after the crystallization time was beyond 7 h. In addition, as shown in Fig. 6a, the hysteresis loops at  $P/P_0 > 0.45$  became smaller with the secondary crystallization time, suggesting that Pd/S-1 is re-crystallized in the process of constructing ZSM-5 shell.

The influences of the shell on the acidity of Pd/S-1 were evaluated by  $NH_3$ -TPD. As shown in the Fig. 7, Pd/S-1 just has weak acid sites, originating from silanol groups on the surface of S-1. In contrast, all the

Pd/S-1@HZSM-5-x samples display significant ammonia desorption peaks contributed by the acidic ZSM-5 shell over Pd/S-1, in which the peaks at around 200 °C and 380 °C are corresponding to the weak and strong acid sites, respectively. From the integrated areas of the desorption peaks, it can be seen that the strong acid amounts on Pd/S-1@HZSM-5-x samples increase with the secondary crystallization time and basically is proportional to coverage of the shell over Pd/S-1 (Table 1). These results indicate that the strong acid amount around Pd NPs is related with the shell coverage and can be tuned by the controlling the secondary crystallization time.

### 3.2. Catalytic performance

Naphthalene hydrogenation was employed as the model reaction to evaluate the hydrogenation performances of the prepared core-shell catalysts, and the reaction scheme is presented in Scheme 1. Under the employed reaction conditions, S-1 and HZSM-5 were inactive in the absence of Pd (Table 3). The catalytic performances of the core-shell catalysts with the different shell coverage for the naphthalene hydrogenation are shown in Fig. 8. Pd/S-1 shows just 5.1 % of naphthalene conversion at 6 h and remains basically below 5% with the reaction time. It is intriguing that Pd/S-1@HZSM-5-x samples exhibit much stronger hydrogenation abilities than Pd/S-1, and their activities increase with the shell integrity. The naphthalene conversion reaches 98.3 % at 6 h over Pd/S-1@HZSM-5-48 with a completely integrated shell and no significant decrease is observed with the reaction time. Pd/S-1@HZSM-5-48 has slightly lower Pd content than Pd/S-1 due to the presence of ZSM-5 shell. Furthermore, the chemical states of the Pd NPs on the two samples are similar. Therefore, the enhancement in hydrogenation ability over Pd/S-1@HZSM-5-48 is closely related to the acidity of the ZSM-5 shell. This can be confirmed by the gradually enhanced activities with the coverage of nano-ZSM-5 over Pd/S-1. For Pd/S-1@HZSM-5-x samples, the increase in ZSM-5 shell coverage boosts the acid amounts around Pd NPs, which are beneficial for spillover

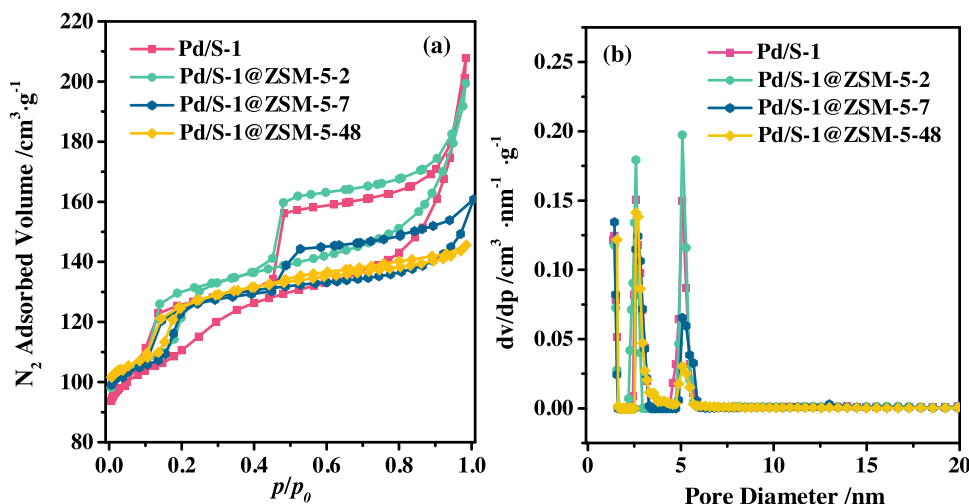


Fig. 6.  $N_2$  adsorption-desorption isotherms (a) and pore size distribution (b) of different samples.

Table 2

Textural properties of the different samples.

Samples	Si/Al Atomic ratios <sup>a</sup>	Pd loading <sup>a</sup> (wt%)	$S_{BET}^b$ ( $m^2/g$ )	$S_{micro}^b$ ( $m^2/g$ )	$S_{meso}^b$ ( $m^2/g$ )	$V_{total}^b$ ( $cm^3/g$ )	$V_{meso}^b$ ( $cm^3/g$ )
S-1	–	–	426.4	387.9	38.5	0.21	0.04
Pd/S-1	–	1.0	417.2	307.1	110.1	0.28	0.14
Pd/S-1@ZSM-5-2	133.5	0.71	426.8	323.1	103.7	0.26	0.13
Pd/S-1@ZSM-5-7	99.8	0.67	434.3	364.7	69.6	0.25	0.09
Pd/S-1@ZSM-5-48	94.8	0.65	442.3	372.5	69.8	0.23	0.07
Pd/S-1@ZSM-5-96	92.1	0.64	429.0	368.5	60.5	0.22	0.06

<sup>a</sup> Determined by ICP.

<sup>b</sup> Determined by  $N_2$  adsorption.

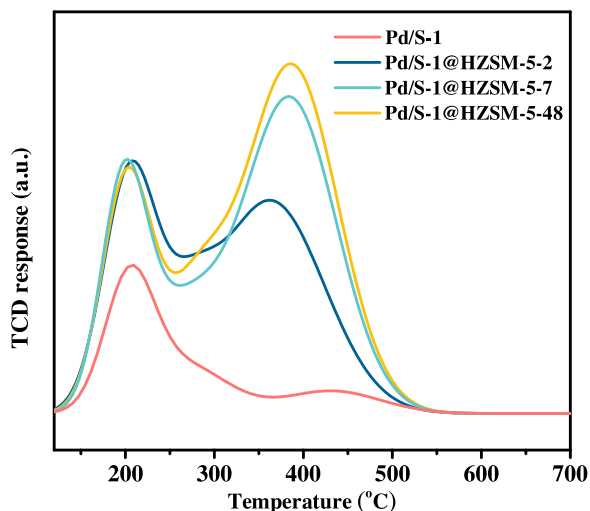


Fig. 7.  $NH_3$ -TPD profiles of the different samples.

hydrogenation. Hence, the acid induced spillover hydrogenation is the main factor for the enhancement in hydrogenation ability over Pd/S-1@HZSM-5-48.

In order to confirm this, Pd/S-1@NaZSM-5-48 was prepared by ion-exchange with NaCl solution, and its catalytic performance was also evaluated in naphthalene hydrogenation. As expected, Pd/S-1@NaZSM-5-48 has much lower hydrogenation ability than Pd/S-1@HZSM-5-48, and the naphthalene conversion is just 27.7 % (Table 3).  $NH_3$ -TPD measurement shows that Pd/S-1@NaZSM-5-48 displays the ammonia desorption peaks from the weak and medium acid sites at range from

Table 3

Catalytic behaviors of the different reference catalysts in naphthalene hydrogenation.

Entry	Catalysts	Conversion (%)	Selectivity (%)	
			Tetralin	Decalin
1	S-1	–	–	–
2	HZSM-5	–	–	–
3	Pd/S-1	4.3	100	0
4	Pd/S-1@HZSM-5-48	96.1	94.8	5.2
5	Pd/S-1@NaZSM-5-48	27.7	97.6	2.4
6	Pd/S-1@HZSM-5-48-1	57.6	97.8	2.2
7	Pd/S-1@HZSM-5-48-2	95.8	88.6	11.4
8	Pd/[S-1@HZSM-5-48]	71.5	96.2	3.8
9	Pd/HZSM-5	77.4	95.7	4.3
10	Pd/S-1+HZSM-5	8.8	99.8	0.2
11	Pd/S-1@HZSM-5-96	61.2	98.2	1.8

(Reaction conditions: WHSV:  $1.3 h^{-1}$ ,  $H_2$ /feed:750, 4 MPa  $H_2$ , 280 °C, time on stream:10 h).

200 to 350 °C (Figure S3), while the one from the strong acid sites is absent. Combined with the reaction and characterization results, it can be deduced that the strong acid sites on ZSM-5 shell play a vital role in enhanced hydrogenation ability of Pd/S-1. To further illustrate this point, two Pd/S-1@HZSM-5-48 samples were synthesized in the synthesis system with  $SiO_2/Al_2O_3$  ratios of 126 and 45, respectively (Figure S4). Even if it is difficult to accurately measure the Si/Al ratios in the shell, for the different core shell catalysts, the Si/Al ratios determined by ICP also can reflect the acidity of the constructing shell. Pd/S-1@HZSM-5-48-1 with a Si/Al ratio of 147 shows a lower hydrogenation activity than Pd/S-1@HZSM-5-48. In contrast, Pd/S-1@HZSM-5-48 with a Si/Al ratio of 72 shows the similar naphthalene conversion and slightly higher selectivity to decalin than Pd/S-1@HZSM-5-48 with a

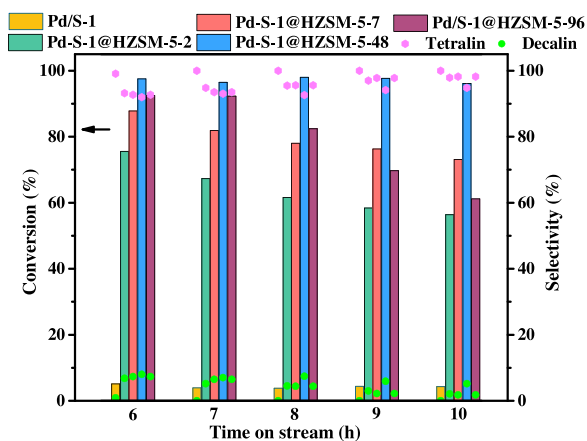


**Fig. 8.** Catalytic performances of naphthalene hydrogenation over different core-shell catalysts. (Reaction conditions: WHSV = 1.3 h<sup>-1</sup>, H<sub>2</sub>/feed = 750, 4 MPa H<sub>2</sub>, 280 °C).

Si/Al ratio of 94.8. This can be ascribed to less/more strong acid amount on Pd/S-1@HZSM-5-48-1/-2 than on Pd/S-1@HZSM-5-48 (Figure S5). The above results further demonstrate that the strong acid sites of Pd/S-1@ZSM-5 core-shell catalyst play an important role for enhancing hydrogenation ability.

To reveal the structural features of the prepared core-shell catalyst in naphthalene hydrogenation, the following control experimental were done. First, Pd/[S-1@HZSM-5-48] were prepared by wet impregnation method using S-1@HZSM-5-48 as the support and Na<sub>2</sub>PdCl<sub>4</sub> as Pd precursor. Even if Pd/[S-1@HZSM-5-48] has the similar Pd loading, and strong acid amounts to Pd/S-1@HZSM-5-48, it shows the lower hydrogenation ability than Pd/S-1@HZSM-5-48 (Table 3). The different catalytic performances obtained over the two catalysts can be ascribed to the different positions of Pd NPs on the two catalysts. In naphthalene hydrogenation, reaction substrate naphthalene (0.703 × 0.907 nm) is hard to diffuse into the ZSM-5 channel (0.51 × 0.55 and 0.52 × 0.58 nm), thus, naphthalene hydrogenation over the samples prepared mainly occurs on the Pd NPs/acid sites located on the external surface of supports. In the case of Pd/S-1@HZSM-5-48, all Pd NPs was covered all round by the nano-ZSM-5 shell, while not all Pd NPs can be covered by nano-ZSM-5 shell for Pd/[S-1@HZSM-5-48]. This may cause the acid amount with a proximity to Pd NPs on Pd/S-1@HZSM-5-48 is more than on Pd/[S-1@HZSM-5-48]. Second, Pd/HZSM-5 was prepared by impregnating Na<sub>2</sub>PdCl<sub>4</sub> on HZSM-5, and the prepared Pd/HZSM-5 has a similar Pd loading and acid amount to Pd/S-1@HZSM-5-48 (Figure S3). As shown in Table 3, the hydrogenation activity of Pd/HZSM-5 was lower than Pd/S-1@HZSM-5-48. Pd NPs in Pd/HZSM-5 were mainly located on the external surface of HZSM-5, while the acid sites are mainly on the surface of the channel wall, thus, the accessible acid sites with proximity to supported Pd NPs were limited, resulting in lower hydrogenation ability of Pd/HZSM-5. Third, Pd/S-1+HZSM-5 was prepared by mixing Pd/S-1 with HZSM-5. The chosen HZSM-5 has a similar Si/Al ratio, morphology (hexagonal) and particle size to the HZSM-5 coated on Pd/S-1 (Figure S6), thus the acid amount accessible to naphthalene is also approximate for Pd/S-1@HZSM-5-48 and Pd/S-1+HZSM-5 two samples. However, Pd/S-1+HZSM-5 gives much lower naphthalene conversion (below 10 %) than Pd/S-1@HZSM-5-48. This is mainly due to the poor proximity between Pd NPs and the accessible acid sites, which is unfavorable for acid induced spillover hydrogenation. These results further demonstrate that the enhanced hydrogenation ability over Pd/S-1@HZSM-5-48 is closely related to the accessible acid amounts with proximity to Pd NPs. Apart from this, the nano-ZSM-5 shell in Pd/S-1@HZSM-5-48 also plays a vital role in observed catalytic performance of Pd/S-1@HZSM-5-48 in naphthalene hydrogenation. Pd/S-1@HZSM-5-96 with a dense ZSM-5 shell was prepared by

**Table 4**  
Sulfur tolerance tests of the core-shell catalysts.

Catalysts	Thionaphthene-containing	Conversion (%)	Selectivity (%)	
			Tetralin	Decalin
Pd/S-1@HZSM-5-48	0	96.1	94.8	5.2
Pd/S-1@HZSM-5-48	500	73.9	95.4	4.6
Pd/[S-1@HZSM-5-48]	0	71.5	96.2	3.8
Pd/[S-1@HZSM-5-48]	500	39.5	98.1	1.9

(Reaction conditions: WHSV:1.3 h<sup>-1</sup>, H<sub>2</sub>/feed:750, 4 MPa H<sub>2</sub>, 280 °C, time on stream:10 h).

prolonging the crystallization time (Figure S6). As shown in Table 3, it can be seen that Pd/S-1@HZSM-5-96 shows the lower hydrogenation ability than Pd/S-1@HZSM-5-48 even it has more strong acid sites (Figure S3). Thus, the ZSM-5 nanocrystal shells in Pd/S-1@HZSM-5-48 show superior structural features than other supported Pd catalysts for naphthalene hydrogenation.

### 3.3. Sulfur-tolerant tests

The sulfur-tolerant performances of Pd/[S-1@HZSM-5-48] and Pd/S-1@HZSM-5-48 were evaluated in the presence of thionaphthene. As shown in Table 4, the naphthalene conversions over both two catalysts decrease to some extent. However, Pd/S-1@HZSM-5-48 in sulfur-tolerant test still keep 76.8 % of its original activity at time on stream of 10 h, while Pd/[S-1@HZSM-5-48] drops to its 55.2 % of the original activity at identical time on stream. These results indicate that Pd/S-1@HZSM-5-48 has better sulfur tolerance ability than Pd/[S-1@HZSM-5-48]. This can be explained by the reason that the acidic nano-ZSM-5 shells can protect the Pd NPs from poisoning by organic sulfide to some extent.

## 4. Conclusion

In summary, an efficient Pd/S-1@ZSM-5 core-shell catalyst with enhanced hydrogenation ability was designed and prepared via epitaxial growth. The nano-ZSM-5 shell coverage increases with the extension of crystallization time. Meanwhile, the strong acid amounts of Pd/S-1@ZSM-5 core-shell catalyst also increase. Pd/S-1@HZSM-5 core-shell catalysts exhibit stronger hydrogenation capacity for naphthalene hydrogenation, which greatly attributed to increase of strong acid amounts around Pd NPs and rational structural design of nano-ZSM-5 shell. The strong acid sites of Pd/S-1@ZSM-5 core-shell catalyst play a decisive role for enhancing hydrogenation ability. Moreover, Pd/S-1@ZSM-5 core-shell catalyst also shows good sulfur-tolerance for naphthalene hydrogenation in the present of thionaphthene. The core-shell provides a new alternative way for constructing high-efficient noble metal hydrogenation catalysts.

### CRedit authorship contribution statement

**Ningyue Lu:** Conceptualization, Validation, Writing - original draft. **Jiaxin Zhao:** Investigation. **Qi Dong:** Methodology. **Yanpeng Zhao:** Validation. **Binbin Fan:** Supervision, Funding acquisition, Writing - review & editing.

### Declaration of Competing Interest

The authors declare no conflict of interest.

### Acknowledgments

This work was supported by the National Natural Science Foundation of China (No. 21576177) and Shanxi Provincial Key Research and Development Projects (No. 201903D121036).

## Appendix A. Supplementary data

Supplementary material related to this article can be found, in the online version, at doi:<https://doi.org/10.1016/j.mcat.2021.111543>.

## References

- [1] A. Stanislaus, B.H. Cooper, Aromatic hydrogenation catalysis: a review, *Catal. Rev.* 36 (1994) 75–123.
- [2] M. Zahmakıran, Y. Tonbul, S. Ozkar, Ruthenium (0) nanoclusters stabilized by a nanozeolite framework: isolable, reusable, and green catalyst for the hydrogenation of neat aromatics under mild conditions with the unprecedented catalytic activity and lifetime, *J. Am. Chem. Soc.* 132 (2010) 6541–6549.
- [3] S. Miao, Z. Liu, B. Han, J. Huang, Z. Sun, J. Zhang, T. Jiang, Ru nanoparticles immobilized on montmorillonite by ionic liquids: a highly efficient heterogeneous catalyst for the hydrogenation of benzene, *Angew. Chem.* 118 (2006) 272–275.
- [4] B. Pawelec, R. Mariscal, R.M. Navarro, S.V. Bokhorst, S. Rojas, J.L.G. Fierro, Hydrogenation of aromatics over supported Pt-Pd catalysts, *Appl. Catal. A Gen.* 225 (2002) 223–237.
- [5] L. Zhu, S. Shan, V. Petkov, W. Hu, A. Kroner, J. Zheng, C. Yu, N. Zhang, Y. Li, R. Luque, C.-J. Zhong, H. Ye, Z. Yang, B.H. Chen, Ruthenium–nickel–nickel hydroxide nanoparticles for room temperature catalytic hydrogenation, *J. Mater. Chem. A Mater. Energy Sustain.* 5 (2017) 7869–7875.
- [6] M. Pang, C. Liu, W. Xia, M. Muhler, C. Liang, Activated carbon supported molybdenum carbides as cheap and highly efficient catalyst in the selective hydrogenation of naphthalene to tetralin, *Green Chem.* 14 (2012) 1272.
- [7] Y. Cheng, H. Fan, S. Wu, Q. Wang, J. Guo, L. Gao, B. Zong, B. Han, Enhancing the selectivity of the hydrogenation of naphthalene to tetralin by high temperature water, *Green Chem.* 11 (2009) 1061–1065.
- [8] B.H. Cooper, B.B.L. Donniss, Aromatic saturation of distillates: an overview, *Appl. Catal. A Gen.* 137 (1996) 203–223.
- [9] C. Song, A.D. Schmitz, Zeolite-supported Pd and Pt catalysts for low-temperature hydrogenation of naphthalene in the absence and presence of benzothiophene, *Energy Fuel* 11 (1997) 656–661.
- [10] T. Tang, C. Yin, L. Wang, Y. Ji, F. Xiao, Good sulfur tolerance of a mesoporous Beta zeolite-supported palladium catalyst in the deep hydrogenation of aromatics, *J. Catal.* 257 (2008) 125–133.
- [11] M. Du, Z. Qin, H. Ge, X. Li, Z. Lü, J. Wang, Enhancement of Pd–Pt/Al<sub>2</sub>O<sub>3</sub> catalyst performance in naphthalene hydrogenation by mixing different molecular sieves in the support, *Fuel Process. Technol.* 91 (2010) 1655–1661.
- [12] K. Cheng, J. Kang, S. Huang, Z. You, Q. Zhang, J. Ding, W. Hua, Y. Lou, W. Deng, Y. Wang, Mesoporous Beta zeolite-supported ruthenium nanoparticles for selective conversion of synthesis gas to C<sub>5</sub>–C<sub>11</sub> isoparaffins, *ACS Catal.* 2 (2012) 441–449.
- [13] K. Na, N. Musselwhite, X. Cai, S. Alayoglu, G.A. Somorjai, Promotional effects of mesoporous zeolites with Pt nanoparticle catalysts during reforming of methylcyclopentane, *J. Phys. Chem. A* 118 (2014) 8446–8452.
- [14] S.A. D'Ippolito, A.D. Ballarini, C.L. Pieck, Influence of support acidity and Ir content on the selective ring opening of Decalin over Ir/SiO<sub>2</sub>–Al<sub>2</sub>O<sub>3</sub>, *Energy Fuel* 31 (2017) 5461–5471.
- [15] M.A. Arribas, P. Concepción, A. Martínez, The role of metal sites during the coupled hydrogenation and ring opening of tetralin on bifunctional Pt(Ir)/USY catalysts, *Appl. Catal. A Gen.* 267 (2004) 111–119.
- [16] T. He, Y. Wang, P. Miao, J. Li, J. Wu, Y. Fang, Hydrogenation of naphthalene over noble metal supported on mesoporous zeolite in the absence and presence of sulfur, *Fuel* 106 (2013) 365–371.
- [17] X. Meng, Y. Wu, Y. Li, Tailoring the pore size of zeolite Y as the support of diesel aromatic saturation catalyst, *J. Porous Mater.* 13 (2006) 365–371.
- [18] T. Tang, C. Yin, L. Wang, Y. Ji, F. Xiao, Superior performance in deep saturation of bulky aromatic pyrene over acidic mesoporous Beta zeolite-supported palladium catalyst, *J. Catal.* 249 (2007) 111–115.
- [19] H. Chen, H. Yang, O. Omotoso, L. Ding, Y. Briker, Y. Zheng, Z. Ring, Contribution of hydrogen spillover to the hydrogenation of naphthalene over diluted Pt/RHO catalysts, *Appl. Catal. A Gen.* 358 (2009) 103–109.
- [20] S.D. Lin, M.A. Vannice, Hydrogenation of aromatic hydrocarbons over supported Pt catalysts. I. Benzene hydrogenation, *J. Catal.* 143 (1993) 539–553.
- [21] S.D. Lin, M.A. Vannice, Hydrogenation of aromatic hydrocarbons over supported Pt catalysts. II. Toluene hydrogenation, *J. Catal.* 143 (1993) 554–562.
- [22] S.D. Lin, M.A. Vannice, Hydrogenation of aromatic hydrocarbons over supported Pt catalysts. III. Reaction models for metal surfaces and acidic sites on oxide supports, *J. Catal.* 143 (1993) 563–572.
- [23] S. Lee, K. Lee, J. Im, H. Kim, M. Choi, Revisiting hydrogen spillover in Pt/LTA: effects of physical diluents having different acid site distributions, *J. Catal.* 325 (2015) 26–34.
- [24] J. Im, H. Shin, H. Jang, H. Kim, M. Choi, Maximizing the catalytic function of hydrogen spillover in platinum-encapsulated aluminosilicates with controlled nanostructures, *Nat. Commun.* 5 (2014) 3370.
- [25] J. Liu, H. Zhang, N. Lu, X. Yan, B. Fan, R. Li, Influence of acidity of mesoporous ZSM-5-supported Pt on naphthalene hydrogenation, *Ind. Eng. Chem. Res.* 59 (2020) 1056–1064.
- [26] Z.-Q. Li, X. Fu, C. Gao, J. Huang, B. Li, Y. Yang, J. Gao, Y. Shen, Z. Peng, J.-H. Yang, Z. Liu, Enhancing the matching of acid/metal balance by engineering an extra Si–Al framework outside the Pd/HBeta catalyst towards benzene hydroalkylation, *Catal. Sci. Technol.* 10 (2020) 1467–1476.
- [27] J. Zhang, L. Wang, B. Zhang, H. Zhao, U. Kolb, Y. Zhu, L. Liu, Y. Han, G. Wang, C. Wang, D.S. Su, B.C. Gates, F.-S. Xiao, Sinter-resistant metal nanoparticle catalysts achieved by immobilization within zeolite crystals via seed-directed growth, *Nat. Catal.* 1 (2018) 540–546.
- [28] J. Zhang, L. Wang, Y. Shao, Y. Wang, B.C. Gates, F.-S. Xiao, A Pd@zeolite catalyst for nitroarene hydrogenation with high product selectivity by sterically controlled adsorption in the zeolite micropores, *Angew. Chem. Int. Ed.* 129 (2017) 9747–9751.
- [29] N. Wang, Q. Sun, J. Yu, Ultrasmall metal nanoparticles confined within crystalline nanoporous materials: a fascinating class of nanocatalysts, *Adv. Mater.* 31 (2019), 1803966.
- [30] J. Wang, L. Liu, X. Dong, L. Alfilfil, C.-E. Hsiung, Z. Liu, Y. Han, Converting hierarchical to bulk structure: a strategy for encapsulating metal oxides and noble metals in zeolites, *Chem. Mater.* 30 (2018) 6361–6369.
- [31] T.L. Cui, W.Y. Ke, W.B. Zhang, H.H. Wang, X.H. Li, J.S. Chen, Encapsulating palladium nanoparticles inside mesoporous MFI zeolite nanocrystals for shape-selective catalysis, *Angew. Chem. Int. Ed.* 55 (2016) 9178–9182.
- [32] H.J. Cho, D. Kim, J. Li, D. Su, B. Xu, Zeolite-Encapsulated Pt nanoparticles for tandem catalysis, *J. Am. Chem. Soc.* 140 (2018) 13514–13520.
- [33] N. Wang, Q. Sun, R. Bai, X. Li, G. Guo, J. Yu, In situ confinement of ultrasmall Pd clusters within nanosized Silicalite-1 zeolite for highly efficient catalysis of hydrogen generation, *J. Am. Chem. Soc.* 138 (2016) 7484–7487.
- [34] Z. Jin, L. Wang, E. Zuidema, K. Mondal, M. Zhang, J. Zhang, C. Wang, X. Meng, H. Yang, C. Mesters, F.S. Xiao, Hydrophobic zeolite modification for in situ peroxide formation in methane oxidation to methanol, *Science* 367 (2020) 193–197.
- [35] Q. Sun, B.W.J. Chen, N. Wang, Q. He, A. Chang, C.M. Yang, H. Asakura, T. Tanaka, M.J. Hulsey, C.H. Wang, J. Yu, N. Yan, Zeolite-encaged Pd-Mn nanocatalysts for CO<sub>2</sub> hydrogenation and formic acid dehydrogenation, *Angew. Chem. Int. Ed.* 59 (2020) 20183–20191.
- [36] S. Song, V. Fung Kin Yuen, L. Di, Q. Sun, K. Zhou, N. Yan, Integrating Biomass into the Organonitrogen Chemical Supply Chain: Production of Pyrrole and d-Proline from Furfural, *Angew. Chem. Int. Ed.* 59 (2020) 19846–19850.
- [37] C. Wang, E. Guan, L. Wang, X. Chu, Z. Wu, J. Zhang, Z. Yang, Y. Jiang, L. Zhang, X. Meng, B.C. Gates, F.S. Xiao, Product selectivity controlled by nanoporous environments in zeolite crystals enveloping rhodium nanoparticle catalysts for CO<sub>2</sub> hydrogenation, *J. Am. Chem. Soc.* 141 (2019) 8482–8488.
- [38] Y. Chai, S. Liu, Z.-J. Zhao, J. Gong, W. Dai, G. Wu, N. Guan, L. Li, Selectivity modulation of encapsulated Palladium nanoparticles by zeolite microenvironment for biomass catalytic upgrading, *ACS Catal.* (2018) 8578–8589.
- [39] H. Cho, D. Kim, S. Li, D. Su, D. Ma, B. Xu, Molecular level proximity of metal and acid sites in zeolite encapsulated Pt nanoparticles for selective multistep tandem catalysis, *ACS Catal.* 10 (2019) 3340–3348.
- [40] M. Moliner, J.E. Gabay, C.E. Kiewer, R.T. Carr, J. Guzman, G.L. Casty, P. Serna, A. Corma, Reversible transformation of Pt nanoparticles into single atoms inside high-silica chabazite zeolite, *J. Am. Chem. Soc.* 138 (2016) 15743–15750.
- [41] Z. Wu, S. Goel, M. Choi, E. Iglesia, Hydrothermal synthesis of LTA-encapsulated metal clusters and consequences for catalyst stability, reactivity, and selectivity, *J. Catal.* 311 (2014) 458–468.
- [42] S. Goel, Z. Wu, S.I. Zones, E. Iglesia, Synthesis and catalytic properties of metal clusters encapsulated within small-pore (SOD, GIS, ANA) zeolites, *J. Am. Chem. Soc.* 134 (2012) 17688–17695.
- [43] S. Goel, S.I. Zones, E. Iglesia, Encapsulation of metal clusters within MFI via interzeolite transformations and direct hydrothermal syntheses and catalytic consequences of their confinement, *J. Am. Chem. Soc.* 136 (2014) 15280–15290.
- [44] X. Yang, Q. Liu, Y. Zhang, X. Su, Y. Huang, T. Zhang, In situ synthesis of metal clusters encapsulated within small-pore zeolites via a dry gel conversion method, *Nanoscale* 10 (2018) 11320–11327.
- [45] Y. Chen, X. Wang, L. Zhang, A strategy for fast and facile embedding platinum nanoparticles in silicalite-1 crystallites with a stable and catalytic active structure, *Chem. Eng. J.* 394 (2020), 124990.
- [46] M. Javed, S. Cheng, G. Zhang, P. Dai, Y. Cao, C. Lu, R. Yang, C. Xing, S. Shan, Complete encapsulation of zeolite supported Co based core with silicalite-1 shell to achieve high gasoline selectivity in Fischer-Tropsch synthesis, *Fuel* 215 (2018) 226–231.
- [47] J. Přech, D.R. Strossi Pedrollo, N.R. Marcilio, B. Gu, A.S. Peregodova, M. Mazur, V. V. Ordonsky, V. Valtchev, A.Y. Khodakov, Core-Shell metal zeolite composite catalysts for in situ processing of Fischer-Tropsch hydrocarbons to gasoline type fuels, *ACS Catal.* 10 (2020) 2544–2555.
- [48] C. Liu, L. Lin, Y. Cao, H. Liu, Y. Guo, X. Zhang, Amino-functionalized seeds-induced synthesis of encapsulated Pd@Silicalite-1 core-shell catalysts for size-selective hydrogenation, *Catal. Commun.* 109 (2018) 16–19.
- [49] H. Tao, H. Yang, Y. Zhang, J. Ren, X. Liu, Y. Wang, G. Lu, Space-confined synthesis of nanorod oriented-assembled hierarchical MFI zeolite microspheres, *J. Mater. Chem. A Mater. Energy Sustain.* 1 (2013) 13821.